 SDHM, vol.8, no.3, pp.223-247, 2012

Crack Growth Modelling in Functionally Graded Materials by Mesh-Free Method

P.H. Wen[1] **and M.H. Aliabadi**[2]

Abstract: A mesh-free method for modelling crack growth in functionally graded materials is presented. Based on the variational principle of the potential energy, mesh-free method has been implemented with enriched radial bases interpolation functions to evaluate mixed-mode stress intensity factors, which are introduced to capture the singularity of stress at the crack tip. Paris law and the maximum principle stress criterion are adopted for defining the growth rate and direction of the fatigue crack growth respectively. The accuracy of the proposed method is assessed by comparison to other available solutions.

Keywords: Meshless method, stress intensity factors, enriched radial bases functions, fatigue crack growth, Paris law, functionally graded materials.

1 Introduction

In a method for life time prediction of damaged structures, the influence of the geometry of the component or structure and its interaction with the growing crack should be considered. In general, numerical methods such as the Boundary Element Method (BEM) and the Finite Element Method (FEM) are used in the fracture analysis of structures, because of the complex shape and continuously changing path of the growing crack. More recently, Mesh-free (also referred to as Meshfree) methods have grown in popularity. Regardless of the numerical method being used, crack growth incremental analysis requires remeshing at the end of each crack extension. Except for the very simple cases, where the crack paths are known prior, remeshing can be quite cumbersome.

Early attempts to model crack growth using the Finite Element Method (FEM) can be traced back to works of Shepard et al (1985); Tong et al (1973); Soboyejo et al (1990); Remzi and Blackburn (1990). A popular approach to model crack growth

[1] School of Engineering and Materials Science, Queen Mary, University of London, London, UK, E1 4NS

[2] Department of Aeronautics, Imperial College, London, UK, SW7 2BY

is the discrete crack modeling approach (see Kawai (1978); Currtin (1990)). More recent advances in the finite element method can be found in the work of Swift (1992); Theilig et al (1997) for two-dimensional mixed-mode crack problems, and, [11,12,16, 42, 54,55] for three–dimensional mixed-mode problems.

The *enriched element* was developed Benzley (1974) by adding the analytic expression of the crack tip field to the conventional finite elements. The enriched elements formed the immediate layer of elements surrounding the crack-tip. Further progress on enriched elements were reported by Foschi and Barrett (1976); Gifford and Hinton (1978); Heppler and Hansen (1981); Heyliger and Kriz (1989). Hybrid elements developed by Theilig and Buchholz (1999) are similar in concept to the enriched elements, in the sense that both approaches are based on assumed displacement and/or stress distributions near the crack tip and both allow for the direct evaluation of the stress intensity factors as global unknowns. The major difference between the two methods lies in the method of enforcing the inter-element compatibility of displacement variables. The enriched elements use a special transition element, while the hybrid elements typically use a modified variational principle (see [4]).

Another interesting method for modeling crack propagation is the Embedded Finite Element Method (EFEM). A review of EFEM can be found in Jirasek (2000).

A more recent successful application of the FEM to mixed-model crack growth modeling is due to the development of eXtended Finite Element Method (XFEM). The XFEM as developed by Black and Belytscchko (1999); Rethore et al (2005) is inspired by the enriched finite elements originally proposed by Benzley (1974) (see Aliabadi and Rooke (1991) for an overview of enriched FEM).

A robust method for modeling crack growth in general mixed-mode problems was developed by Portela et al (1993); Mi and Aliabadi (1994, 1995). The method is based on the Dual Boundary Element Method earlier proposed by Portela et al (1993); Mi and Aliabadi (1992) as an effective way of modeling crack problems using the boundary integral equation. The DBEM for the first time allowed modeling mixed-mode crack problems without a need for continuous remeshing and user interferences. The crack extension was modeled with new boundary elements without having to remesh the previous crack geometry. The extension of the DBEM to different linear, transient and nonlinear problems can be found in Benedetti et al (2008); Cisilino and Aliabadi (1999, 2004); Dell'Erba and Aliabadi (2000); Dirgantara and Aliabadi (2000); Leitao et al (1995); Prasad et al (1996); Saleh and Aliabadi (1995); Salgado and Aliabadi (1998); Wen and Aliabadi (2011). Another interesting development in 3D crack growth modeling is the coupled symmetric Galerkin boundary element method formulation with FEM alternating method as presented by Han and Atluri (2002). A review of boundary

element methods for crack growth modeling can be found in [2].

During the last decades, mesh-free methods, as an alternative to Finite Element Method (FEM), have shown a promising potential and has found applications on various problems (see Atluri and Zhu (1998); Belytschko et al (1994); Duarte and Oden (1996); Gingold and Monaghan (1977); Liu et al (1995); Nayroles et al (1992)). Among different kinds of mesh-free methods proposed so far, Element free Galerkin and Meshless local Petrov-Galerkin (MLPG) have gained much attention both using Moving least square (MLS) approximation as the shape function construction. More recently, Liu and Gu (1999) introduced a point interpolation method which uses Radial bases (RB) function to construct the shape function. Valliappan and Murti (1985); Wen and Aliabadi (2007, 2008); Wen et al (2011) applied the Radial bases function to analysis of elastodynamic, functionally graded materials and fracture mechanics problems. A new formulation of EFG was proposed by Liu and Gu (1999) through the moving kriging (MK) interpolation in order to eliminate the shortcoming that EFG shape function does not satisfy the Kronecker delta property.

This paper presents a mesh-free method with enriched radial bases function for modelling crack growth for functionally graded materials. An enriched radial bases function has been introduced to catch up the singularity of stresses near crack tip. The crack growth is simulated simply by adding two new nodes, i.e. one node indicates new crack tip and one is split from previous crack tip. Compared with classic finite element method, meshing and re-meshing for crack propagation problems are not necessary in this approach. The incremental crack length is obtained by integrating the Paris law for a given increment of load cycles. The mixed-mode stress intensity factors are evaluated with satisfactory accuracy either by using the J-integral or crack opening displacements. Two numerical examples are presented to demonstrate the validity of the proposed method.

2 Variational principle of potential energy

Consider a homogeneous anisotropic and linear elasticity solid, the relationships between stresses and strains by Hooke's law are given by

$$\sigma_{ij}(\mathbf{x}) = C_{ijkl}(\mathbf{x})\varepsilon_{kl}(\mathbf{x}) = C_{ijkl}(\mathbf{x})u_{k,l}(\mathbf{x}), \tag{1}$$

where$\varepsilon_{kl} = (u_{k,l} + u_{l,k})/2,$ and C_{ijkl} denotes the elasticity tensor which has the following symmetries

$$C_{ijkl} = C_{jikl} = C_{klij}. \tag{2}$$

For a homogeneous isotropic solid, we have

$$C_{ijkl}(\mathbf{x}) = \lambda(\mathbf{x})\delta_{ij}\delta_{kl} + \mu(\mathbf{x})\left(\delta_{ik}\delta_{jl} + \delta_{il}\delta_{jk}\right) \tag{3}$$

where λ and μ are the Lame's constants, which are functions of coordinates $\mathbf{x}$ in general case. For the orthotropic plane-strain state, Hooke's law can also be written, in matrix form, as

$$\boldsymbol{\sigma} = \begin{Bmatrix} \sigma_{11} \\ \sigma_{11} \\ \sigma_{11} \end{Bmatrix} = \mathbf{D} \begin{Bmatrix} \varepsilon_{11} \\ \varepsilon_{22} \\ \varepsilon_{12} \end{Bmatrix} = \mathbf{D}\boldsymbol{\varepsilon} \tag{4}$$

where

$$\mathbf{D}(\mathbf{y}) = \frac{E(\mathbf{y})[1-\nu(\mathbf{y})]}{[1+\nu(\mathbf{y})][1-2\nu(\mathbf{y})]} \begin{bmatrix} 1 & \frac{\nu(\mathbf{y})}{1-\nu(\mathbf{y})} & 0 \\ \frac{\nu(\mathbf{y})}{1-\nu(\mathbf{y})} & 1 & 0 \\ 0 & 0 & \frac{1-2\nu(\mathbf{y})}{2[1-\nu(\mathbf{y})]} \end{bmatrix} \tag{5}$$

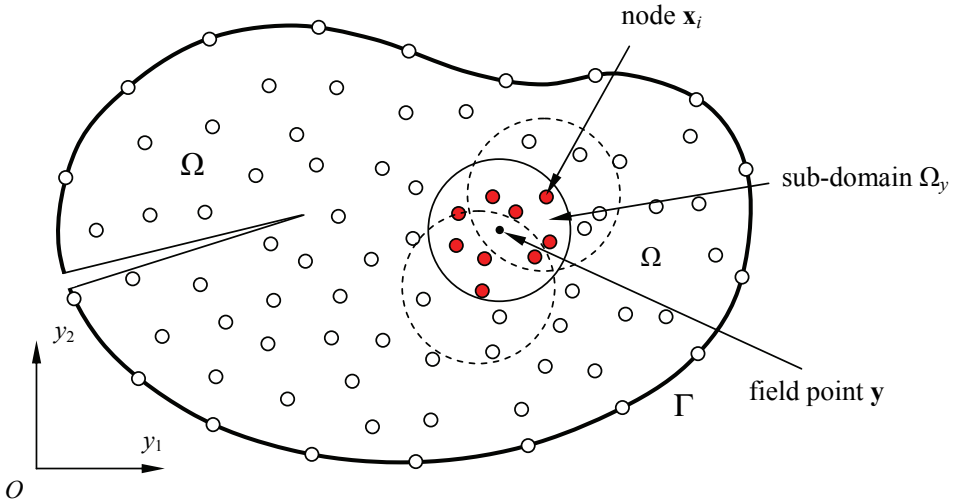

Figure 1: Support domain Ω_y for RBF interpolation of the field point $\mathbf{y}$ in a cracked body.

in which, $E(\mathbf{y})$ is the Young's modulus and $\nu\acute{I}(\mathbf{y})$ the Poisson's ratio. Both them are functions of the position of analysis point. With the shape functions, the displacements $\mathbf{u}(\mathbf{y})$ at the point $\mathbf{y}$ can be approximated in terms of the nodal values in

a local domain (see Figure 1), called as support domain, as

$$u_i(\mathbf{y}) = \sum_{k=1}^{n} \phi_k(\mathbf{y},\mathbf{x}_k)\hat{u}_i^k = \bar{\blacksquare}(\mathbf{y},\mathbf{x})\hat{\mathbf{u}}_i \tag{6}$$

where

$$\bar{\mathbf{\Phi}}(\mathbf{y},\mathbf{x}) = \{\phi_1(\mathbf{y},\mathbf{x}_1), \phi_2(\mathbf{y},\mathbf{x}_2), ..., \phi_n(\mathbf{y},\mathbf{x}_n)\} \tag{7}$$

and the nodal value

$$\hat{\mathbf{u}}_i = \left\{\hat{u}_i^1, \hat{u}_i^2, ..., \hat{u}_i^n\right\}^{\mathrm{T}},\ i = 1,2 \tag{8}$$

at point $\mathbf{x}_k = \left\{x_1^{(k)}, x_2^{(k)}\right\}$, where $k = 1,2,...,n(\mathbf{y})$, ϕ_k the shape function and $n(\mathbf{y})$ the number of nodes in the local supported domain. For the two dimensional elasticity, we can rearrange the above relation in a matrix form as

$$\mathbf{u}(\mathbf{y}) = \{u_1, u_2\}^{\mathrm{T}} = \blacksquare(\mathbf{y},\mathbf{x})\hat{\mathbf{u}} \tag{9}$$

$$\mathbf{\Phi}(\mathbf{y},\mathbf{x}) = \begin{bmatrix} \bar{\mathbf{\Phi}} & 0 \\ 0 & \bar{\mathbf{\Phi}} \end{bmatrix} = \begin{bmatrix} \phi_1 & 0 & \phi_2 & 0 & ... & \phi_n & 0 \\ 0 & \phi_1 & 0 & \phi_2 & ... & 0 & \phi_n \end{bmatrix} \tag{10}$$

$$\hat{\mathbf{u}} = \left\{\hat{u}_1^1, \hat{u}_2^1, \hat{u}_1^2, \hat{u}_2^2 ..., \hat{u}_1^n, \hat{u}_2^n\right\}^{\mathrm{T}} \tag{11}$$

Therefore, the relationship between strains and displacements is given by

$$\boldsymbol{\varepsilon}(\mathbf{y}) = \begin{bmatrix} \frac{\partial\phi_1}{\partial y_1} & 0 & \frac{\partial\phi_2}{\partial y_1} & 0 & ... & \frac{\partial\phi_n}{\partial y_1} & 0 \\ 0 & \frac{\partial\phi_1}{\partial y_2} & 0 & \frac{\partial\phi_2}{\partial y_2} & ... & 0 & \frac{\partial\phi_n}{\partial y_2} \\ \frac{\partial\phi_1}{\partial y_2} & \frac{\partial\phi_1}{\partial y_1} & \frac{\partial\phi_2}{\partial y_2} & \frac{\partial\phi_2}{\partial y_1} & ... & \frac{\partial\phi_n}{\partial y_2} & \frac{\partial\phi_n}{\partial y_1} \end{bmatrix} \hat{\mathbf{u}} = \mathbf{B}(\mathbf{y},\mathbf{x})\hat{\mathbf{u}}. \tag{12}$$

Considering the variation of the total potential energy, with respect to each nodal displacement yields $2\times N$ a linear algebraic equation system in a matrix form as

$$[\mathbf{K}]_{2N\times 2N}\,\hat{\mathbf{u}}_{2N} = \mathbf{f}_{2N} \tag{13}$$

where N is the number of node in the domain $\Omega_{,}$ and on the boundary. The stiffness and mass matrices can be written as

$$\mathbf{K} = \int_{\Omega} \mathbf{B}^{\mathrm{T}}(\mathbf{y},\mathbf{x})\mathbf{D}(\mathbf{y})\mathbf{B}(\mathbf{y},\mathbf{x})d\Omega(\mathbf{y}) \tag{14}$$

for nodes $\mathbf{x} = \mathbf{x}_i$ $i = 1, 2, ...N$, and nodal force vector is defined by

$$\mathbf{f} = \int_{\Omega} \mathbf{\Phi}^{\mathrm{T}}(\mathbf{y}, \mathbf{x}) \mathbf{b}(\mathbf{y}) d\Omega(\mathbf{y}) + \int_{\Gamma_\sigma} \mathbf{\Phi}^{\mathrm{T}}(\mathbf{y}, \mathbf{x}) \mathbf{t}(\mathbf{y}) d\Gamma(\mathbf{y}) \tag{15}$$

where $\mathbf{b} = \{b_1, b_2\}^{\mathrm{T}}$ is the vector of body force, vector of traction $\mathbf{t} = \{t_1, t_2\}^{\mathrm{T}}$, in which $t_i = \sigma_{ij} n_j$, n_i denotes a unit outward normal vector, σ denotes the boundary on which the traction is given. For a concentrated force acting at node i, we may determine the nodal force vector directly by

$$\mathbf{f}_i = \left\{ F_1^i, F_2^i \right\}^{\mathrm{T}} \tag{16}$$

3 The approximation scheme

A sub-domain Ω_y as shown in Figure 1 is introduced in a neighbourhood of point $\mathbf{y}$ and is defined as local support domain. In order to guarantee unique solution of the interpolation problem, the distribution of function u in the sub-domain Ω_y over a number of randomly distributed notes $\{\mathbf{x}_i\}$, $i = 1, 2, ..., n(\mathbf{y})$ is interpolated by

$$u(\mathbf{y}) = \sum_{k=1}^{n} R_k(\mathbf{y}, \mathbf{x}) a_k + \sum_{j=1}^{t} P_j(\mathbf{x}) b_j = \mathbf{R}(\mathbf{y}, \mathbf{x}) \mathbf{a} + \mathbf{P}(\mathbf{y}) \mathbf{b} \tag{17}$$

along with the constraints

$$\sum_{j=1}^{n} P_k(\mathbf{x}_j) a_j = 0, \quad 1 \le k \le t \tag{18}$$

where $\{P_k\}_{k=1}^{t}$ is a bases for P_{m-1}, the set of devariate polynomials of degree $\le m-1$, and

$$t = \binom{m+d-1}{d}$$

is the dimension of P_{m-1}. A set of linear equations can be written, in the matrix form, as

$$\mathbf{R}_0 \mathbf{a} + \mathbf{P} \mathbf{b} = \hat{\mathbf{u}}, \quad \mathbf{P}_0^T \mathbf{a} = \mathbf{0} \tag{19}$$

where matrix

$$\mathbf{R}_0(\mathbf{x}, \mathbf{x}) = \begin{bmatrix} R(\mathbf{x}_1, \mathbf{x}_1) & R(\mathbf{x}_1, \mathbf{x}_2) & ... & R(\mathbf{x}_1, \mathbf{x}_n) \\ R(\mathbf{x}_2, \mathbf{x}_1) & R(\mathbf{x}_2, \mathbf{x}_2) & ... & R(\mathbf{x}_2, \mathbf{x}_n) \\ . & . & ... & . \\ . & . & ... & . \\ . & . & ... & . \\ R(\mathbf{x}_n, \mathbf{x}_1) & R(\mathbf{x}_n, \mathbf{x}_2) & ... & R(\mathbf{x}_n, \mathbf{x}_n) \end{bmatrix} \tag{20}$$

and

$$\mathbf{P}_0(\mathbf{x}) = \begin{bmatrix} P_1(\mathbf{x}_1) & P_2(\mathbf{x}_1) & \dots & P_t(\mathbf{x}_1) \\ P_1(\mathbf{x}_2) & P_2(\mathbf{x}_2) & \dots & P_t(\mathbf{x}_2) \\ . & . & \dots & . \\ . & . & \dots & . \\ . & . & \dots & . \\ P_1(\mathbf{x}_n) & P_2(\mathbf{x}_n) & \dots & P_t(\mathbf{x}_n) \end{bmatrix} \tag{21}$$

Solving (19) gives

$$\mathbf{b} = \left(\mathbf{P}_0^T \mathbf{R}_0^{-1} \mathbf{P}_0\right)^{-1} \mathbf{P}_0^T \mathbf{R}_0^{-1} \hat{\mathbf{u}}, \quad \mathbf{a} = \mathbf{R}_0^{-1} \left[\mathbf{I} - \mathbf{P}_0 \left(\mathbf{P}_0^T \mathbf{R}_0^{-1} \mathbf{P}_0\right)^{-1} \mathbf{P}_0^T \mathbf{R}_0^{-1}\right]^{\hat{\mathbf{u}}} \tag{22}$$

where $\mathbf{I}$ denotes the diagonal unit matrix. To capture singular stresses at crack tip, enriched radial bases function has been selected as following

$$R_k(\mathbf{y},\mathbf{x}) = R(y,x) = \sqrt{c^2 + |\mathbf{y} - \mathbf{x}_k|^2} + \sqrt{r}\, e^{-\alpha r} \tag{23}$$

where $r = |\mathbf{y} - \mathbf{y}_c|$; c and α are free parameters; $\mathbf{y}_c$ $(y_1^{(c)}, y_2^{(c)})$ denotes the location of the crack tip. Substituting the coefficients $\mathbf{a}$ and $\mathbf{b}$ from (22) into (23), we can obtain the approximation of the field function in terms of the nodal values

$$u_i(\mathbf{y}) = \left\langle \mathbf{R}(\mathbf{y},\mathbf{x}) \mathbf{R}_0^{-1} \left[\mathbf{I} - \mathbf{P}\left(\mathbf{P}^T \mathbf{R}_0^{-1} \mathbf{P}\right)^{-1} \mathbf{P}^T \mathbf{R}_0^{-1}\right] + \mathbf{P}(\mathbf{y}) \left(\mathbf{P}^T \mathbf{R}_0^{-1} \mathbf{P}\right)^{-1} \mathbf{P}^T \mathbf{R}_0^{-1} \right\rangle \hat{\mathbf{u}}$$
$$= \sum_{k=1}^{n} \phi_k(\mathbf{y}) \hat{u}_i^k \tag{24}$$

where $\mathbf{R}(\mathbf{y},\mathbf{x}) = \{R_1(\mathbf{y},\mathbf{x}_1), R_2(\mathbf{y},\mathbf{x}_2), ..., R_n(\mathbf{y},\mathbf{x}_n)\}$ and $\mathbf{P}(\mathbf{y}) = \left\{1, y_1, y_2, y_1^2, y_1 y_2, y_2^2 ...\right\}$ are a set of radial bases functions centred around the point $\mathbf{y}$ and the set of devariate polynomials respectively. It is worth noting that this shape function depends uniquely on the distribution of scattered nodes within the support domain and it has the property of the Kronecker Delta function. In addition, the inverse matrix of coefficient $\mathbf{R}_0^{-1}(\mathbf{x})$ depend on the distribution of the node $\mathbf{x}_i$ located in the support domain only, therefore it is easy to evaluate the first and higher order derivatives of shape function from Equation (10). From Equation (17), we have

$$u_{i,j}(\mathbf{y}) = \sum_{k=1}^{n} \phi_{k,j} \hat{u}_i^k \; i = 1,2 \tag{25}$$

From Equation (23), we have

$$R_{k,j}(\mathbf{y},\mathbf{x}_k) = \frac{y_j - x_j^{(k)}}{\sqrt{c^2 + |\mathbf{y} - \mathbf{x}_k|^2}} + \frac{y_j - y_j^{(c)}}{r} \left(\frac{1}{2\sqrt{r}} - \alpha\sqrt{r}\right) e^{-\alpha r} \; j = 1,2. \tag{26}$$

$$\mathbf{P}_{,1}(\mathbf{y}) = \{0,\ 1,\ 0, 2y_1\ , y_2,\ 0, ...\} \tag{27}$$

$$\mathbf{P}_{,2}(\mathbf{y}) = \{0,\ 0,\ 1,\ 0,\ y_1,\ 2y_2, ...\} \tag{28}$$

Therefore, the first order derivative for displacements is of $1/\sqrt{r}$ singularities at crack tip. In addition, the introduction of the polynomial terms has very slight effect on the accuracy (see Wen and Aliabadi (2011), therefore we have, $\mathbf{a} = \mathbf{R}_0^{-1}\hat{\mathbf{u}}$ and $\mathbf{b} = \mathbf{0}$ simply.

4 Fatigue crack growth analysis

To evaluate stress intensity factors, both J-integral and crack opening displacement (COD) are used in this paper. For a mixed-mode fracture problem and constant material properties, the stress intensity factors are related with the J-integral for plane-strain as following

$$\frac{1-\nu^2(\mathbf{y}_c)}{E(\mathbf{y}_c)}\left(K_{\mathrm{I}}^2 + K_{\mathrm{II}}^2\right) = J \tag{29}$$

where $J = \int\limits_{\Gamma'} \left(Wn_1 - t_\beta u_{\beta,1}\right) d\Gamma'$ and Γ' is an arbitrary closed contour, oriented in the anti-clockwise direction, starting from the lower crack surface to the upper one and incorporating the crack tip and $W = \sigma_{\alpha\beta}\varepsilon_{\alpha\beta}/2$is strain energy density in the field. Alternatively stress intensity factors for plane strain problem, can be obtained from

$$K_{\mathrm{I}} = \frac{E(\mathbf{y}_c)}{8[1-\nu^2(\mathbf{y}_c)]}\sqrt{\frac{2\pi}{r_0}}\Delta u_2,\ K_{\mathrm{II}} = \frac{E(\mathbf{y}_c)}{8[1-\nu^2(\mathbf{y}_c)]}\sqrt{\frac{2\pi}{r_0}}\Delta u_1 \tag{30}$$

where r_0 indicates the distance between calculation point on the crack surface and the crack tip. Obviously for the functionally graded materials, the arbitrary closed contour or the distance r_0 should be small enough in order that the material properties can be considered as constants. It is worth noting that in the evaluation of J-integral, the coordinate system should be a local system, i.e. direction 1 is along the direction of crack growth. As there are two variables in equation (29), we need to introduce another equation. A simple procedure based on the decomposition of the elastic field into its respective symmetric and anti-symmetric mode composites, can be used to separate the stress intensity factors of a mixed-mode problem, see Kitagawa et al (1976); Rigby and Aliabadi (1998). However, the simplest and most direct way is to introduce the ratio of the crack opening displacements (COD), i.e. $\psi(r_0) = \Delta u_2/\Delta u_1$, therefore the mixed-mode stress intensity factors

can be evaluated by

$$K_{\mathrm{I}} = \sqrt{\frac{E(\mathbf{y}_c)J}{[1-\nu^2(\mathbf{y}_c)](1+\psi^2)}},\ K_{\mathrm{II}} = \psi K_{\mathrm{I}} \tag{31}$$

where a circle of radius r_0 centred at the crack tip is selected to be a J-integral contour. In general case, the crack path is a smooth curved path. However, crack propagation is simulated by successive linear increments, which direction needs to be determined. Several criteria have been proposed to describe the local direction of mixed-mode crack growth (see Aliabadi and Rooke (1991); Erdogan and Sih (1963); Sih (1974)). The maximum principal stress criterion Erdogan and Sih (1963) is adopted in this paper. This criterion postulates that the growth of crack will occur in a direction perpendicular to the maximum principal stress (the minor principal direction at the crack tip). Thus, at each crack tip, the local direction of crack growth is determined by the condition that the shear stress is zero, that is

$$K_{\mathrm{I}} \sin\theta_c + K_{\mathrm{II}}(3\cos\theta_c - 1) = 0 \tag{32}$$

$$\theta_c = 2\arctan\left[\left(\psi \pm \sqrt{\psi^2+8}\right)/4\right] \tag{33}$$

Obviously the direction of crack growth depends on the ration ψ only near the crack tip. The equivalent stress intensity factor is defined for the mixed-mode fracture as follows

$$K_{\mathrm{eq}}(a) = K_{\mathrm{I}}\cos^3\frac{\theta_c}{2} - 3K_{\mathrm{II}}\cos^2\frac{\theta_c}{2}\sin\frac{\theta_c}{2} \tag{34}$$

and the growth rate of crack are computed by the generalized Paris' law

$$\frac{da}{dN} = C\Delta K_{\mathrm{eq}}^m(a) \tag{35}$$

where $\Delta K_{\mathrm{eq}} = (1-R)K_{\mathrm{eq,max}}$, $R = K_{\mathrm{eq},mix}/K_{\mathrm{eq,max}} = \sigma_{\min}/\sigma_{\max}$, C and m are empirical constants characteristic of the material. The constant m, Paris constant, is typically in the range 3-4 for common steal and aluminum alloys. At the end of each incremental analysis, the equivalent stress intensity factors are calculated and the number of cycles ΔN_i necessary to growth an arbitrary crack-extension increment size $\Delta a$is obtained by

$$\Delta N_i = \frac{1}{C}\int_{a_i}^{a_i+\Delta a} \Delta K_{\mathrm{eq}}^{-m}(a)da. \tag{36}$$

The implementation of this method can be carried out according to the following processes:

1. Choose a finite number of nodes N in the domain Ω and on the boundary;
2. Select crack tip with extra nodes around the crack tip;
3. Divide domain Ω into sub-domain for integration;
4. Loop over integral in sub domain m (m=1,2,...,M) centred at $\mathbf{y}_m$
5. Loop over Gaussian integration points $\mathbf{y}_l$ for each cell,
6. Loop over all nodes in the support domain (i, j);
7. Calculate the shape function $\phi_i(\mathbf{y}, \mathbf{x}_i)$ and first derivative $\phi_{i,k}(\mathbf{y}, \mathbf{x}_i)$;
8. Evaluate the elements $\Delta\mathbf{K}_l^m = \left[a_{kl}^l\right]_{ij}$ with enriched radial bases function;
9. Assemble the system stiffness matrix $\mathbf{K}_{(I,J)}$;
10. End the node loop in the local domain,
11. End the Gaussian point loop,
12. End the cell-integral loop,
13. Introduce the displacement boundary condition solve the system equations;
14. Determine the stress intensity factors and direction of crack growth
15. Go to (ii) or next step;
16. Calculate the cycle number for each crack growth.

5 Numerical examples

5.1 Fatigue crack growth for a single edge slant crack

The rectangular plate (10cm$\times$ 20cm) containing an inclined edge crack (2cm) with an angle 40^0 studied in this example. In this case, we assume the material properties are constants in the domain. A constant cyclic tension in the range from 0 to 40MPa is applied on the top and bottom side of the plate. The material properties are: $E = 74$GPa, $\nu = 0.3$, $C = 19.932 \times 10^{-12}$m / (MN / m$^{1.5}$)^m, $m = 3.32$ and $K_c =$ 60MN / m$^{1.5}$. There are 21$\times$41 uniformly distributed nodes in the domain and 17 extra nodes around the crack tip as shown in Figure 2. Furthermore, in the system stiffness matrix $\mathbf{K}$ in equation.(13), the integral function has a strong singularity of $O(1/r)$ at crack tip. We use polar coordinate to cancel this singularity in the integral

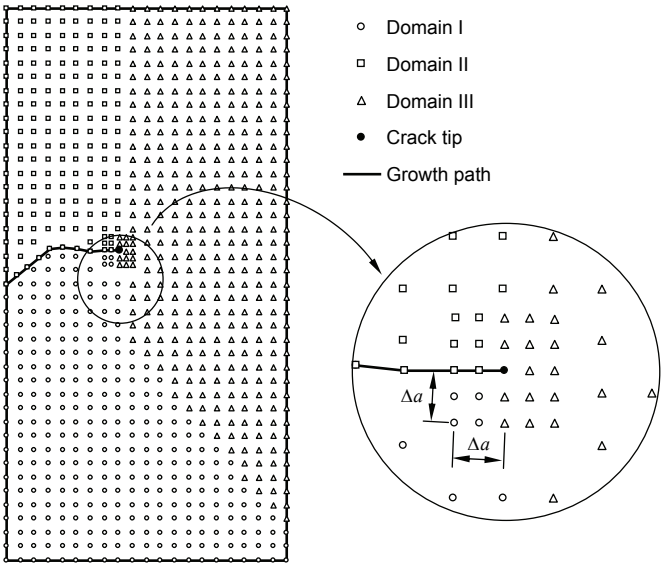

Figure 2: Distribution of the nodes and extra 17 nodes around the crack tip.

function over sub region shown in Figure 3(a). The radius of the circle around the crack tip R_0 is selected in the region between Δa and $3\Delta a$, where Δa represents the increment of crack length, which is selected to 5mm in this example. The radius of the support domain $r_y$centered at field point $\mathbf{y}$ is determined such that the minimum number of nodes in the support domain $n(\mathbf{y}) = 8$. One of two free parameters c is selected as $\eta\Delta a$ and $\eta = 1$. The influence of the second free parameter α (in the radial bases function) on the cycle number and stress intensity factors will be investigated. The integration is performed on 40×80 cells with 4×4 Gauss points in each cell.

Due to the discontinuities of displacement and traction between upper and lower crack surfaces, the traditional support domain such as a circular domain is not valid for the mixed-mode fracture problems. In this example, the cracked body is divided into three sub-domains as illustrated in Figure 2 around the crack tip. Domains I and II, which collocate on the two sides of crack surface, must be uncoupled as the discontinuities of displacements due to crack. Different shapes of supported domain for internal integral points are presented in Figure 2. Therefore, the discontinuity of displacement can be described properly using the radial bases functions. For example, if the calculation point (solid dot in Figure 3(a)) is in zoom I, the collocation nodes in zoom II should be excluded. In addition, if the calculation point is in zoom III and $y_2 > 0$, the collocation nodes in zoom I should be excluded as

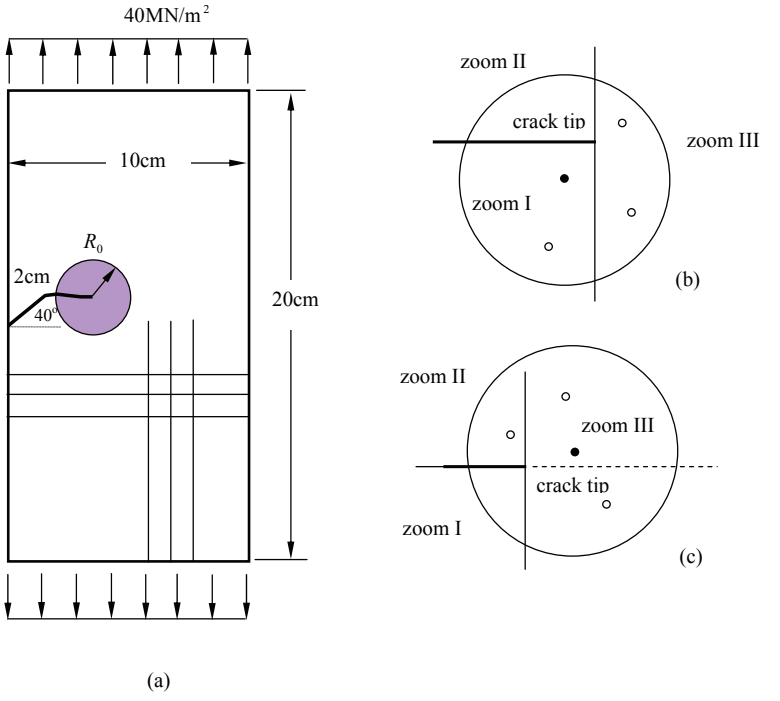

Figure 3: Crack growth in plate and integration area around crack tip. (a): rectangular plate with edge crack; (b) local support domain in zoom I; (c) local support domain in zoom III.

shown in Figure 3(c).

The radius of J-integral contour or the distance between the calculation point and crack tip is chosen as$r_0 = \Delta a$. The J-integral contour is valid for isotropic material only. For the functionally graded materials, there is modification to the integration in (10) (see Sih (1974)). The variation of the stress intensity factors by J-integral technique against the crack length and the fatigue life diagram are presented in Figures 4 and 5 respectively. The initial mode I and mode II SIFs are presented in Table 1. It shows that satisfactory results can be found in the region of α between 1 and 5.

After crack initiates growth, the mode II stress intensity factor tends to zero rapidly. Since the mode II SIF is almost zero for crack propagation, the failure life is dominated by the mode I SIF apart from the initial growth of crack. For the fracture toughness of 60MN / $m^{1.5}$, the maximum crack length failure is found to be 66mm and the failure life is estimated as 139200 cycles by the proposed method with tan-

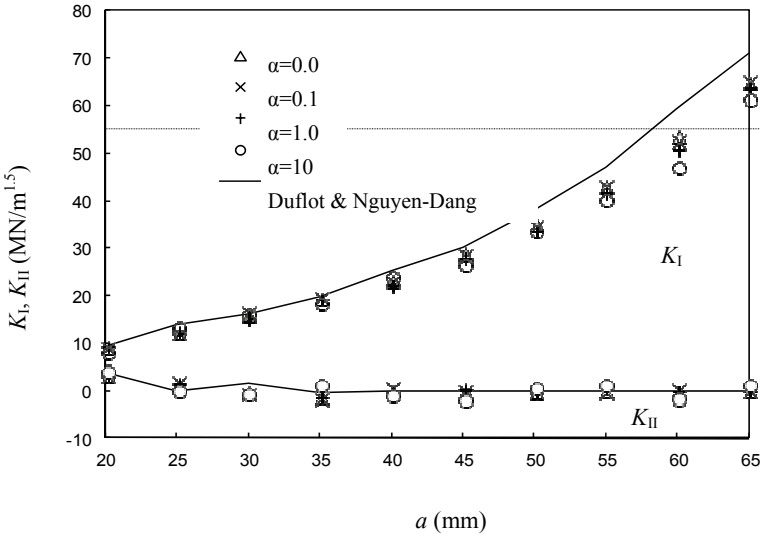

Figure 4: Stress intensity factors vs crack length with different free parameters α.

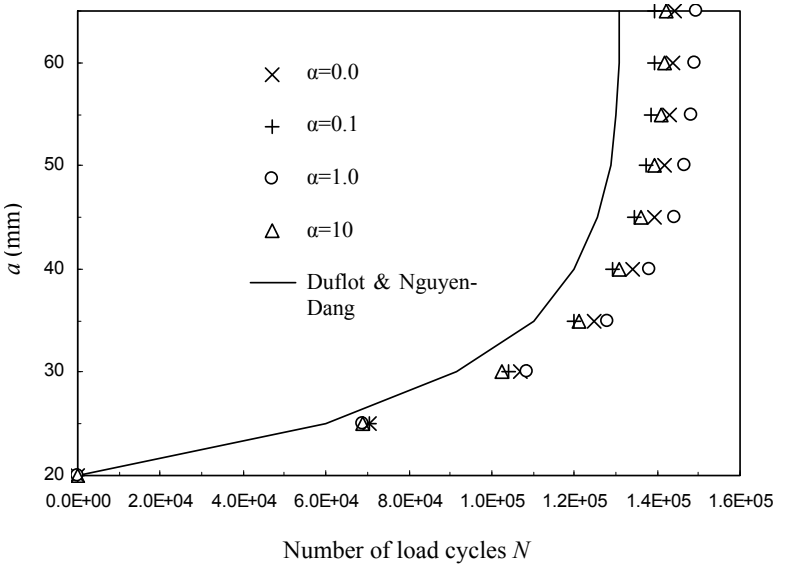

Figure 5: Number of load cycles vs crack length with different free parameters α.

gential technique when α is taken as 1. This is in good agreement with the results by Duflot and Nguyen-Dang (2004): 61.3mm for the final length and 131411 cycles. Figures 4 and 5 show the stress intensity factors $K_{\mathrm{I}}(a)$ and $K_{\mathrm{II}}(a)$ in unit of MN / m$^{1.5}$ against the crack length a (mm) for different selections of a free parameter α. In addition, a sudden change of the direction of the crack growth can be observed at the first increment of the crack length. After that sudden change, the crack growth is almost in a straight line.

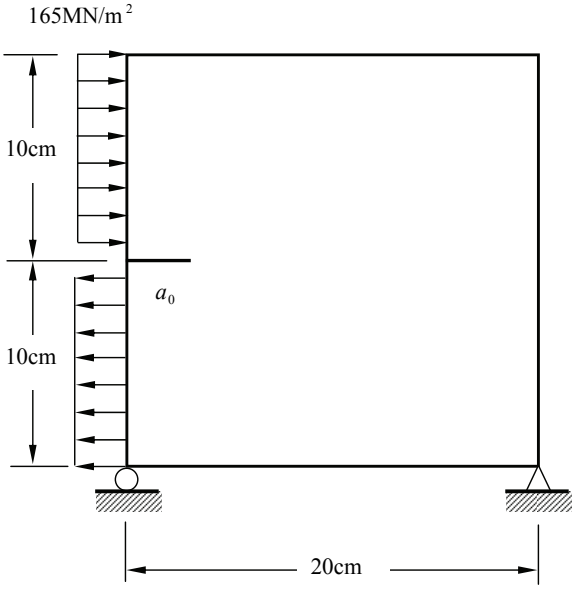

Figure 6: Geometry of a edge cracked square plate under a mode II load.

5.2 A square plate under a mode II fatigue load

A square plate (20cm×20cm) was investigated for a mode II fatigue load by Kim and Lee (2007). Constant cyclic mode II traction in the range from 0 to 165MPa is applied on the upper and lower left edge of the plate in the opposite direction. In this case, 41×41 notes uniformly distribute in the domain and 17 extra nodes around the crack tip as shown in Figure 6. The material properties are: $E = 210$GPa, $\nu = 0.3$, $C = 1.886 \times 10^{-12}$m / (MN / m$^{1.5}$)^m, $m = 3.0$ and $K_c = 200$MN / m$^{1.5}$. The fatigue crack growth is simulated by the tangential technique with crack increment length of 2.5 mm (Δa). The initial crack lengths are specified as 1cm, 2cm, 4cm and 8cm respectively with the same incremental crack growth. The stress intensity

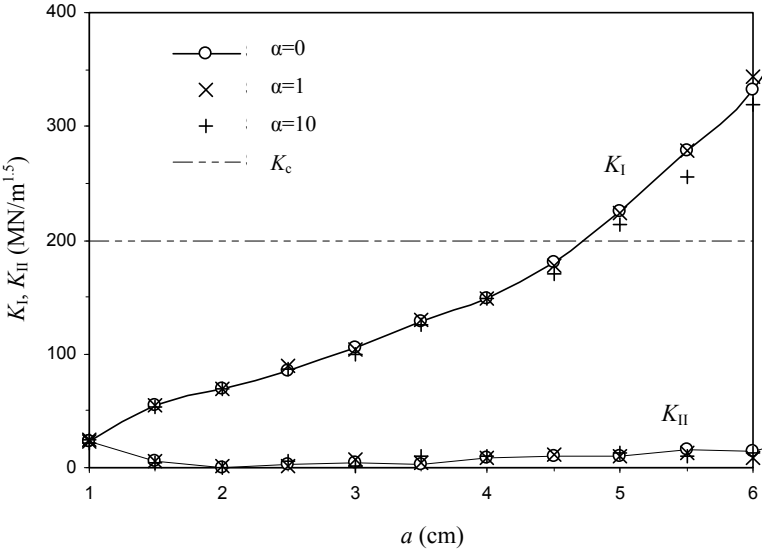

Figure 7: Stress intensity factors vs crack length with different free parameters α.

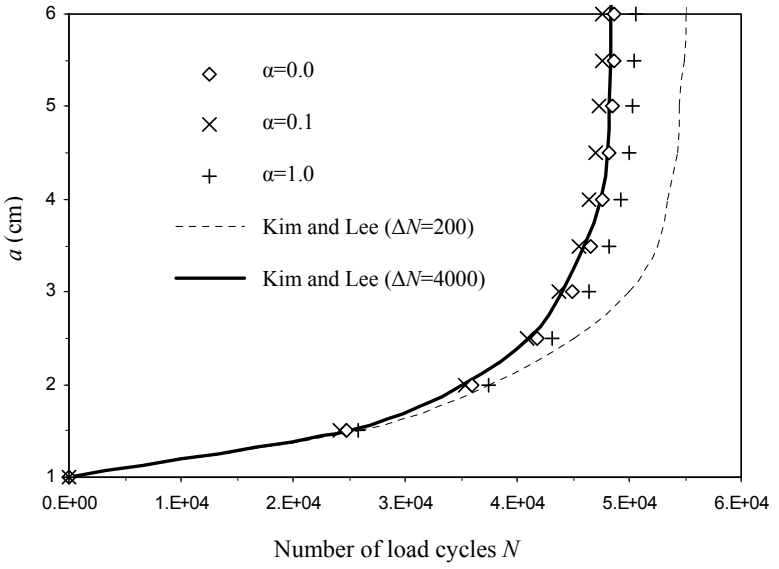

Figure 8: Number of load cycles vs crack length with different free parameters α.

factors$K_{\mathrm{I}}(a)$, $K_{\mathrm{II}}(a)$ in unit of MN/m$^{1.5}$ and the cycling number against the crack length a (mm) are presented with different free parameter α in Figures 7 and 8 respectively. Two different crack increments were used by Kim and (2007) in terms of the increment of cycling number, i.e. $\Delta N = 200$ and $\Delta N = 4000$ respectively. Figure 9 shows the growth paths for these four different initial cracks when free parameter α is taken to 1. In addition, the selection of free parameter α has limited effects on the results of SIFs and the cycling number. Obviously the growth path of the 1cm initial crack forms a sharp curve with a small radius of curvature due to the effect of boundary. In this case, the bending effect dominates the crack propagation direction. Very good agreement has been achieved both for the number of load cycles and crack growth paths with the results given by Kim and (2007) using the boundary element method.

5.3 Functionally graded material cracked square plate under a mode II fatigue load

The plate of same geometry and boundary conditions in *Example 5.2* is investigated for a mode II fatigue load with considering functionally graded materials. Constant cyclic mode II traction with ratio $R = 0$ is applied on the upper and lower left edge of the plate in the opposite direction. It is assumed that Young's modulus E is function of coordinate except Poisson's ratio $\nu(= 0.3)$. In this example, Young's modulus E has an exponential variation in y_1 as

$$E(\mathbf{y}) = E_0 \exp(\beta y_1/b) \tag{37}$$

where $\beta = \ln(E_1/E_0)$, with E_0 and E_1 corresponding to the E-value at $y_1 = 0$ and $y_1 = b$(=20cm) respectively. The nodes are uniformly distributed (41×41) in the domain and 17 extra nodes around the crack tip are used. The fatigue crack growth is simulated using the tangential technique with crack increment length of 2.5 mm (Δa). The initial crack lengths are selected as 1cm and 4cm respectively with the same incremental crack growth. We considered five ratios of $\eta = E_1/E_0$ for each initial crack length, i.e. η equals 0.1, 0.5, 1, 5 and 10 respectively. Crack growth paths for the initial crack length of 1cm are shown in Figures 10 and 11 respectively for each ratio of η. When ratio $E_1/E_0 > 1$, the crack propagation becomes unstable for a large crack length. It is because that the crack tip is too close to the boundary and therefore a fine increment of crack length needs to be introduced. Results by Kim and Lee for constant Young's modulus are presented in the same figure for comparison. In general case, SIF of mode I increases when ratio E_1/E_0 decreases. Similar conclusion can be observed for the initial crack length of 4cm. Growth paths are presented in Figure 12 and all of them are stable for different ratios of young's modulus. Stress intensity factors are plotted in Figure 13 various

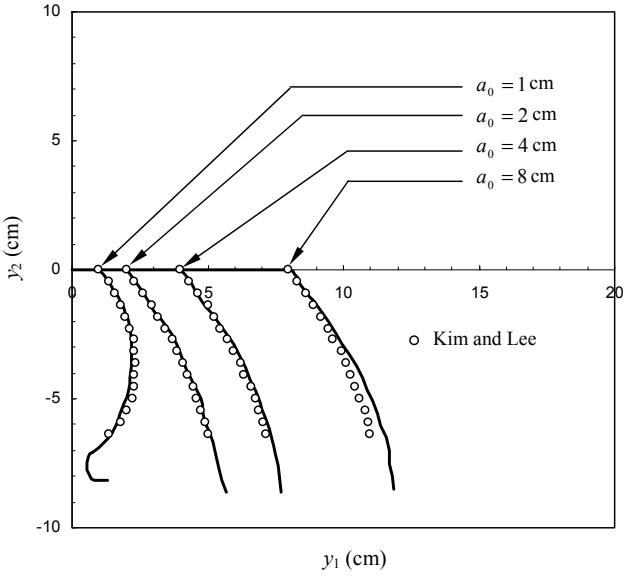

Figure 9: Geometry of a rectangular plate with an edge slant crack: (a) uniform tensile load at the ends; (b) regular distribution of nodes (637); (c) random distribution of nodes (600).

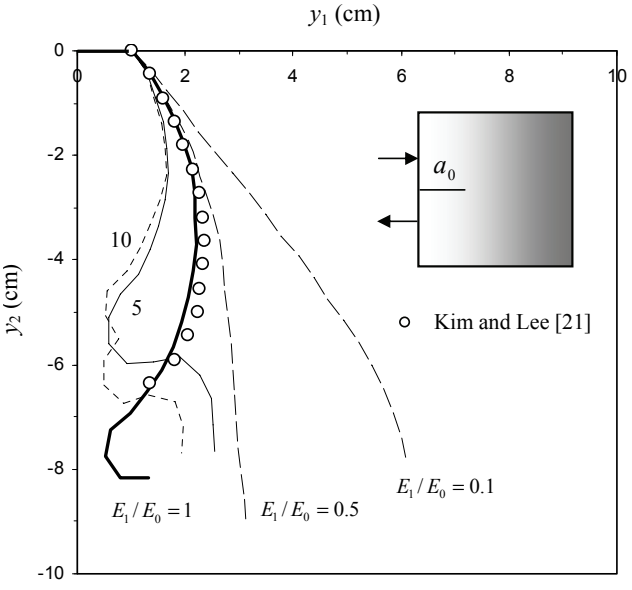

Figure 10: Time dependent normalized stress intensity factors for a rectangular plate with a slant edge crack under tensile step load on the top edge of the plate.

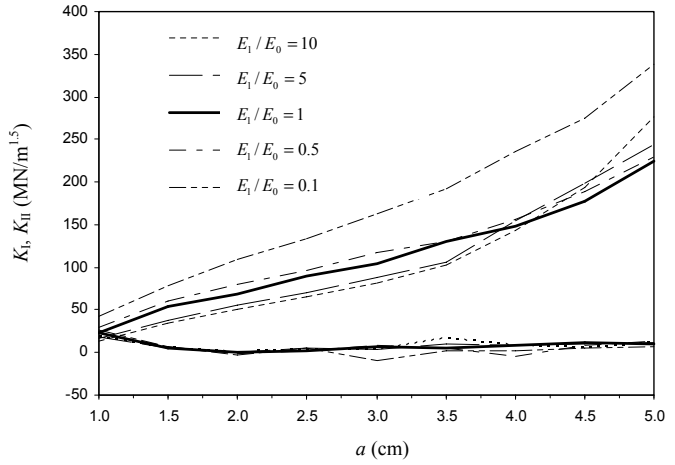

Figure 11: Geometry of a rectangular plate with an edge slant crack: (a) uniform tensile load at the ends; (b) regular distribution of nodes (303); (c) random distribution of nodes (781).

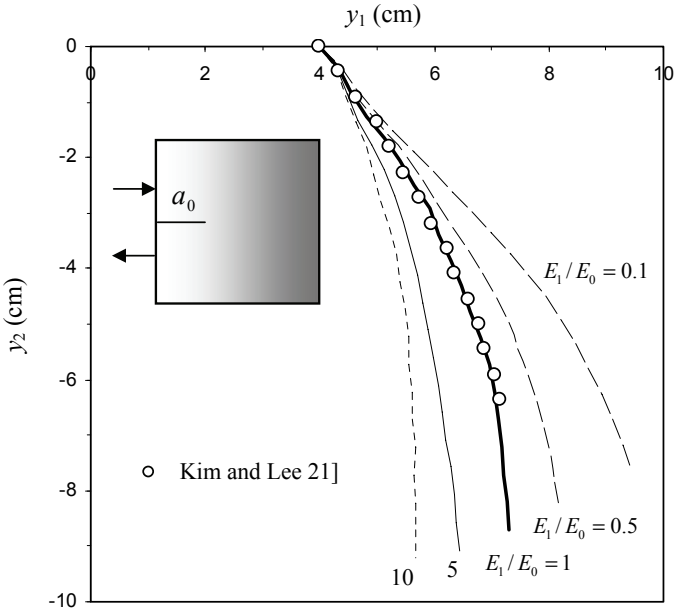

Figure 12: Time dependent normalized stress intensity factors for a rectangular plate with a slant edge crack under tensile step load on the top edge of the plate.

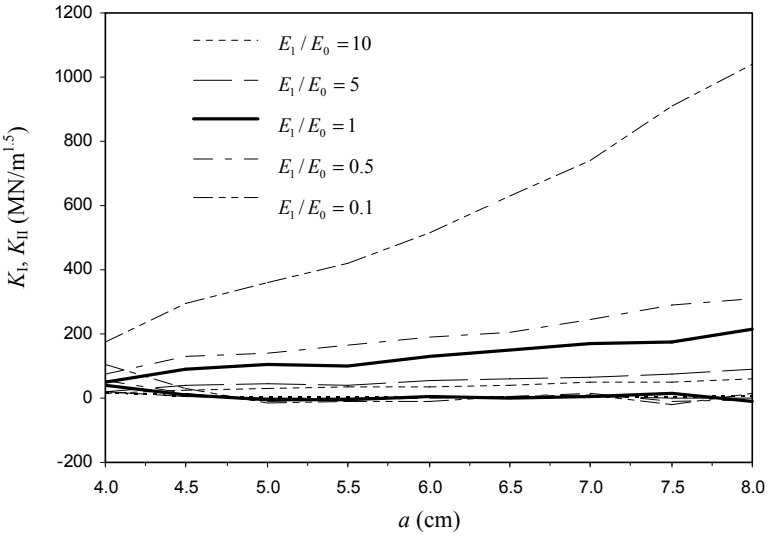

Figure 13: Geometry of a rectangular plate with an edge slant crack: (a) uniform tensile load at the ends; (b) regular distribution of nodes (303); (c) random distribution of nodes (781).

with crack length. In the case of small ratio η, mode I stress intensity factors are increased significantly. Therefore, we can conclude that the functionally graded material has large influence both on crack growth path and stress intensity factors.

6 Conclusion

A mesh-free method for modelling crack growth in functionally graded materials was presented. As shown the method does not require any discretizations of the domain or the boundary. By introducing the enriched RBF interpolation, the singularities of stress in the order of $(1 / \sqrt{r})$ was accurately represented at the crack tip. Three examples of mode I ,mode II and mixed mode were presented. Good agreement was obtained with other published results. Conclusions can be summarised as following:

1. The mesh-free method is efficient for mixed-mode crack propagation problem analysis;

2. The enriched RBFs are flexible and simple to program with little increase in computational efforts;

3. The accuracy of the number of load cycles dependents on the crack increment.

Although this paper analyses the fatigue crack growth for two dimensional edge crack problems, the proposed method can be easily extended to the embedded crack problems and the crack closure problems with friction between two crack surfaces under compressive load.

References

Aliabadi, M.H., Rooke, D.P. (1991): Numerical Fracture Mechanics, WIT Press, Southampton, UK.

Aliabadi, M.H. (1997): A new generation of boundary element methods in fracture mechanics, *Int. J. Fracture*, 86, 91-125.

Aliabadi, M.H., Sollero, P. (1998): Crack growth analysis in homogeneous orthotropic laminates. *Composites Science and Technology*, vol. 58, no. 10, pp. 1697-703.

Atluri, S.N. (1986): *Computational methods in the mechanics of fracture,* vol2, North Holland, Amsterdam.

Atluri, S.N., Zhu, T. (1998): A new meshless local Petrov-Galerkin (MLPG) approach in computational mechanics, *Comput. Mech.*, 22, 117-127.

Atluri, S.N. (2005): Application of DATLE: Damage tolerance analysis and life enhancement [3D non-plannar fatigue crack growth], SID, *Structural Integrity and Durability*, vol. 1, no. 1., pp. 1-20.

Belytschko, T., Lu, Y.Y., Gu, L. (1994) Element-Free Galerkin Methods, *Int. J. Numer. Meth. Engineering*, 37, 229-256.

Benedetti, I., Aliabadi, M.H., Davi, G. (2008): A fast 3D dual boundary element method based on hierarchical matrices. *International Journal of Solids and Structures*, vol. 45, no. 7-8, pp. 2355-76.

Black, T., Belytscchko, T. (1999): Elastic crack growth in finite elements with minimal remeshing, *International Journal for Numerical Methods in Engineering*, vol. 45, pp. 601-620.

Benzley, S.E. (1974): Representation of singularities with isoparametric finite elements, *International Journal for Numerical Methods in Engineering*, vol. 8, pp. 1333-1336

Buchholz, F.G., Richard, H.A. (2004): From Compact Tension Shear (CTS) to All Fracture modes (AFM) Specimen and Loading Devices, *Proc. of the Int. Conf. on Advances in Structural Integrity* (ICASI2004), Bangalore, India.

Buchholz, F.G., Chergui, A., Richard, H.A. (2004): Fracture analyses and experimental results of crack growth under general mixed mode loading conditions. *Engineering Fracture Mechanics*, vol. 71, pp. 455-468.

Cisilino, A.P., Aliabadi, M.H. (1997): Three-dimensional BEM analysis for fatigue crack growth in welded components. *International Journal of Pressure Vessels and Piping*, vol. 70, no. 2, pp. 135-144.

Cisilino, A.P., Aliabadi, M.H. (1999): Three-dimensional boundary element analysis of fatigue crack growth in linear and non-linear fracture mechanics, *Engineering Fracture Mechanics*, vol. 63, pp. 713-733.

Cisilino, A.P., Aliabadi, M.H. (2004): Dual boundary element assessment of three-dimensional fatigue crack growth. *Engineering Analysis with Boundary Elements*, vol. 28, no. 9, pp. 1157-1173.

Cittarella, R., Buchholz F.G. (2007): Comparison of DBEM and FEM crack path predictions with experimental findings for a SEN-specimen under anti-plane shear loading, *Key Engineering Materials*, vols. 348-349, pp. 129-132.

Currtin, W. (1990): Brittle fracture in disordered materials: a spring network model, *J. Material Research*, 5, 535-553.

Dell'Erba, D.N., Aliabadi, M.H. (2000): Three-dimensional thermo-mechanical fatigue crack growth using BEM. *International Journal of Fatigue*, vol. 22, no. 4, pp. 261-273.

Dirgantara, T., Aliabadi, M.H. (2000): Crack growth analysis of plates loaded by bending and tension using dual boundary element method *International Journal of Fracture*, vol. 105, no. 1, pp. 27-47.

Duarte, C.A., Oden, J.T. (1996): An hp adaptive method using clouds, *Compt. Meth. Appl. Mech. Eng.,* 139, 237-262.

Duflot, M., Nguyen-Dang, H. (2004): A meshless method with enriched weight functions for fatigue crack growth, *Int. J. Numerical Methods in Engineering*, 59, 1945-1961.

Erdogan, Sih (1963): On the crack extension in plates under plane loading and transverse shear. *Journal of Basic Engineering,* 86, 519-527.

Fedelinski, P., Aliabadi, M.H., Rooke, D.P. (1997): The time-domain DBEM for rapidly growing cracks *International Journal for Numerical Methods in Engineering*, vol. 40, no. 9, pp. 1555-1572

Foschi, R.O., Barrett, J.D. (1976): Stress intensity factors in anisotropic plates using singular elements, International Journal for Numerical Methods in Engineering, vol. 10, pp. 1281-1287.

Fulland, M., Sander, M., Kullmer, G., Richard, H. A. (2008): Analysis of fatigue crack propagation in the frame of a hydraulic pressure. *Engineering Fracture Mechanics*, vol. 75, pp. 892-900.

Gifford, L.N., Hinton, P.D. (1978): Stress intensity factors by enriched elements, *Engineering Fracture Mechanics*, 10, 485-496.

Gingold, R.A., Monaghan, J.J. (1977): Smooth particle hydrodynamics: theory and applications to non-spherical stars, *Mon. Not. R. Astron. Soc*., 181, 375-389.

Hardy, R.L. (1971): Multiquadric equations of topography and other irregular surfaces, *journal of Geophysical Research*, 76(8), 1905-1915.

Han, Z.D., Atluri, S.N. (2002): SGBEM (for cracked local domain)-FEM (for uncracked global structure) alternating method for analyzing 3D surface cracks and their fatigue-growth, *CMES: Computer Modeling in Engineering and Sciences,* vol. 3, no. 6, pp. 699-716.

Heppler, G., Hansen, J.S. (1981) Mixed-mode fracture analysis of rectilinear anisotropic plates by high order finite elements, *International Journal for Numerical Methods in Engineering*, 17, 445-464.

Heyliger, P.R., Kriz, R.D. (1989) Stress intensity factors by enriched mixed finite elements, *International Journal for Numerical Methods in Engineering*, 28, 1461-1473.

Jirasek, M. (2000): Comparative study on finite elements embedded discontinuities, *Computer Methods in Applied Mechanics and Engineering*, 188, 307-33.

Kim, K., Lee, H. (2007): An incremental formulation for the prediction of two-dimentional fatigue crack growth with curved paths, *Int. J. Numerical Methods in Engineering*, 72, 697-721.

Kitagawa, H., Okamura, H., Ishikawa, H. (1976), Application of J-integral to mixed-mode crack problems, Trans. JSME, 760, 46-48.

Klesnil, M., Lukas, P. (1972): Influence of strength and stress history on growth and stabilisation of fatigue cracks, *Engineering Fracture Mechanics*, vol. 4, pp. 77-92.

Kawai, T. (1978): New discrete models and their application to seismic response analysis of structures, *Nuclear Engineering and Design*, 48, 207-29.

Leis, B.N., Hoper, A.T., Ahmad, J. (1986): Critical review of the fatigue growth of short cracks, *Engineering Fracture Mechanics*, vol. 23, no. 25, pp. 883-898.

Leitao, V.M.A., Aliabadi, M.H., Rooke, D.P. (1995): Elastoplastic simulation of fatigue crack growth dual boundary element formulation *International Journal of Fatigue*, vol. 17, no. 5, pp. 353-363.

Lei Gu (2003) Moving kriging interpolation and element-free Galerkin method, *Int. J. Numer. Meth. Engng,* 56, 1-11.

Linder, C., Armero, F. (2007) Finite elements with embedded strong discontinuities for the modelling of failure in solids, *International Journal for Numerical Methods in Engineering*, 72, 1391-1433.

Liu, W.K., Jun, S., Zhang, Y. (1995) Reproducing kernel particle methods, *Int. J. Numer. Meth. Fluids,* 20, 1081-1106.

Li Q.F., Zhu L., Buchholz F.G., Yan S.Y. (2010): Computational analysis of the AFM specimen on mixed-mode II and III fracture. *Key Engineering Materials*, vols. 452-453, pp. 173-176.

Liu, G.R., Gu, Y.T (1999) A point interpolation method, *in Proc. 4th Asia-Pacific Conference on Computational Mechanics*, 1009-1014.

Mi, Y., Aliabadi, M.H. (1992): Dual boundary element method for three-dimensional fracture mechanics analysis. *Engineering Analysis with Boundary Elements*, vol. 10, no. 2, pp. 161-171.

Mi, Y., Aliabadi, M.H. (1994): Three-dimensional crack growth simulation using BEM *Computers and Structures*, vol. 52, no. 5, pp. 871-878.

Mi, Y., Aliabadi, M.H. (1995): An automatic procedure for mixed-mode crack growth analysis, *Communications in Numerical Methods in Engineering*, vol. 11, no. 2, pp. 167-177.

Nayroles, B., Touzot, G., Villon, P. (1992): Generalizing the finite element method: diffuse approximation and diffuse elements, *Comput. Mech.,* 10, 307-318.

Portela, A., Aliabadi M.H., Rooke D.P. (1993): The dual boundary element method: effective implementation for crack problems. *International Journal for Numerical Methods in Engineering*, vol. 33, no. 6, pp. 1269-87.

Portela, A., Aliabadi, M.H., Rooke, D.P. (1993): Dual boundary element incremental analysis of crack propagation. Computers and Structures, vol. 46, no. 2, pp. 237-247.

Prasad, N.N.V., Aliabadi, M.H., Rooke, D.P. (1996): Thermomechanical fatigue crack growth. *International Journal of Fatigue*, vol. 18, no. 6, pp. 349-361.

Rao, B.N., Rahman, S.A. (2001): Coupled meshless-finite element method for fracture analysis of cracks. *Int. J. Pressure Vessels and Piping* 78, 647-657.

Remzi, E.M., Blackburn, W.S. (1990): Automatic crack propagation studies in T-junction and cross bars. *Engineering Computations,* vol. 7, pp. 116-124.

Rethore, J., Gravouil, A., Combescure (2005): An energy-conserving scheme for dynamic crack growth using the eXtended finite element method. *International Journal for Numerical Methods in Engineering*, vol. 63, pp. 631-659.

Richard, H.A., Linning, W., Henn, K. (1991): Fatigue crack propagation under combined loading. *Forensic Engineering*, vol. 3, no. 2/3, pp. 99-109.

Richard, H.A., Fulland, M., Kullmer, G., Schirmeisen, N. (2010): Experimental and Numerical Investigation of 3D Mixed-Mode Crack Problems in Structures, *SDHM: Structural Durability & Health Monitoring*, 6, 161-188.

Rigby, R., Aliabadi, M.H. (1998): Decompostion of the mixed-mode J-integral-Revisited, *International Journal of Solids and Structures*, 35, 2073-2099.

Saleh, A.L., Aliabadi, M.H. (1995): Crack growth analysis in concrete using boundary element method. *Engineering Fracture Mechanics*, vol. 51, no. 4, pp. 533-545.

Salgado, N.K., Aliabadi, M.H. (1998): Boundary element analysis of fatigue crack propagation in stiffened panels. *Journal of Aircraft*, vol. 35, no. 1, pp. 122-130.

Shepard, M.S., Yehia, N.A.B, Burd, G.S., Weidner, T.J. (1985): Automatic crack propagation tracking. *Computers and Structures*, vol. 20, pp. 211-223.

Silva, L.F.M., Goçalves, J.P.M., Oliveira, F.M.F., de Castro, P.M.S.T. (2000): Multiple-site damage in riveted lap-joints: experimental simulation and finite element prediction. *International Journal of Fatigue*, vol. 22, pp. 319-338.

Sih, G.C. (1974): Strain energy density factor applied to missed mode crack problems, *International Journal of Fracture*, 10, 305-321.

Sladek, J., Sladek, V., Wen, P.H., Aliabadi, M.H. (2006): Meshless Local Petrov-Galerkin (MLPG) method for shear deformable shells analysis. *CMES: Computer Modeling in Engineering & Sciences* 13, 103-117.

Soboyejo, W.O., Knott, J.F., Walsh, M.J., Cropper, K.R. (1990): Fatigue crack propagation of coplanar semi-elliptical cracks in pure bending, *Engineering Fracture Mechanics*, vol. 37, no. 2, pp. 323–40.

Swenson, D.V., Ingraffea, A.R. (1988): Modeling mixed mode dynamic crack propagation using finite elements theory and applications. *Computational Mechanics*, vol 3, pp. 381-397.

Swift, T. (1992): Damage Tolerance Capability, in Specialists Conference on Fatigue of Aircraft Materials, Delft University of Technology.

Theilig, H., Doering, R., Buchholz, F.G. (1997): Higher order fatigue crack path simulation by the MVCCI-method. In B.L. Karihaloo et al (eds), *Advances in Fracture Research*, Pergamon Press, Amsterdam, vol. 4, pp. 2235-2242.

Theilig, H., Buchholz, F.G. (1999): Crack path prediction by MVCCI-method and experimental verification for specimens under proportional bending and shear loading. In C.

Tong, P., Pian, T.H.H., Lasry, S.J. (1973): A hyrid-element approach to crack problems in plane elasticity, *International Journal for Numerical Methods in Engineering*, 7, 297-308.

Valliappan, S., Murti, V. (1985): Automatic remeshing technique in quasi-static and dynamic crack propagation. *Proceddings of the NUMETA, 85 Conference.*, pp 107-116.

Wen, P.H., Aliabadi, M.H. (2007): Meshless method with enriched radial bases functions for fracture mechanics, *SDHM: Structural Durability & Health Monitoring*, 3(2), 107-119.

Wen, P.H., Aliabadi, M.H. (2008): An improved meshless collocation method for elastostatic and elastodynamic problems, *Commun. Numer. Meth. Eng.,* 24, 635-651.

Wen, P.H., Aliabadi, M.H., Liu,Y.W. (2011): Meshless method for crack analysis in functionally graded materials with enriched radial bases functions, *CMES: Computer Modeling in Engineering and Sciences* 30(3), 133-147.

Wen, P.H., Aliabadi, M.H. (2011): A variational approach for evaluation of stress intensity factors using the element free Galerkin method *International Journal of Solids and Structures*, 48, 1171-1179.

Wen, P.H., Aliabadi, M.H., Young, A. (2004): Crack growth analysis for multilayered airframe structures by boundary element method. *Engineering Fracture Mechanics*, vol. 71, no. 4-6, pp. 619-631.

Yagawa, G., Yamada, T. (1996) Free mesh method, a kind of meshless finite element method, *Comput. Mech.,* 18, 383-386.